Inorganic Chemistry
Article

Inorg. Chem. **2010**, *49*, 8763–8768 **8763**
DOI: 10.1021/ic100964j

Phase Transformation and Crystal Structure of $La_2Ni_7H_x$ Studied by in situ X-ray Diffraction

Kenji Iwase,*,†,‡ Kouji Sakaki,† Yumiko Nakamura,† and Etsuo Akiba†

†*National Institute of Advanced Industrial Science and Technology (AIST), AIST Central-5, 1-1-1 Higashi, Tsukuba, Ibaraki 305-8565, Japan, and* ‡*Frontier Research Center of Applied Nuclear Science, Ibaraki University, 162-1 Shirakata, Toukai, Ibaraki 319-1106, Japan*

Received May 13, 2010

The phase transformation of La_2Ni_7 during hydrogenation was investigated by in situ X-ray diffraction. We found two hydride phases, $La_2Ni_7H_{7.1}$ (phase I) and $La_2Ni_7H_{10.8}$ (phase II), during the first absorption cycle. The metal sublattice of phase I was orthorhombic (space group *Pbcn*) with lattice parameters $a = 0.50128(6)$ nm, $b = 0.8702(1)$ nm, and $c = 3.0377(1)$ nm. The sublattice for phase II was monoclinic (space group *C*2/*c*) with lattice parameters $a = 0.51641(9)$ nm, $b = 0.8960(1)$ nm, $c = 3.1289(1)$ nm, and $\beta = 90.17(1)°$. The lattice parameter *c* increased with the hydrogen content, while *a* and *b* decreased in the formation of phase I from the alloy. Phase transformation from phase I to phase II was accompanied by isotropic expansion. The La_2Ni_4 and $LaNi_5$ subunit expanded by 48.9% and 6.0% in volume, respectively, during hydrogenation to phase I. They expanded an additional 14% and 5.8%, respectively, in the formation of phase II. The obtained volume expansion suggested different hydrogen distribution in the La_2Ni_4 and $LaNi_5$ subunit during hydrogenation.

1. Introduction

La and Ni binary compounds with superstructures, $LaNi_3$, La_2Ni_7, and La_5Ni_{19}, have been investigated as candidates for hydrogen storage materials. They consist of cells with $MgZn_2$- and $CaCu_5$-type structures stacking along the *c*-axis in ratios of 1:1 to 1:3. The structural properties of several compounds with $PuNi_3$-, Ce_2Ni_7-, Gd_2Co_7-, and Pr_5Co_{19}-type superstructures have been reported.[1,2] La_2Ni_7 has a hexagonal Ce_2Ni_7-type structure at room temperature and a rhombohedral Gd_2Co_7-type structure at 1249 K.[3,4] These compounds are known to absorb hydrogen, but the hydrogenation and structural properties of their superstructures have not been studied in detail. In this study, we selected Ce_2Ni_7-type La_2Ni_7, which has the highest symmetry among all the La and Ni binary compounds with superstructures, to investigate the structural properties upon hydrogenation.

Oesterreicher et al. reported the hydrogen properties and structures of a series of La−Ni binary compounds.[5] The maximum hydrogen capacity of La−Ni binary compounds increases with the La/Ni ratios: $MgCu_2$-type $LaNi_2$, $PuNi_3$-type $LaNi_3$, and Ce_2Ni_7-type La_2Ni_7 have maximum hydrogen capacities of 1.5, 1.25, and 1.11 H/M, respectively. They become amorphous when hydrogenated at 298 K and 5−10 MPa. Hydrogen-induced amorphization of La_2Ni_7 is promoted above 373 K. A pressure−composition (*P*−*C*) isotherm of La_2Ni_7 was obtained for hydrogen desorption at 323 K, with one sloping plateau present under 0.3 MPa.

Chung et al. reported the crystal structure of hydrogenated La_2Ni_7 using ex situ X-ray diffraction.[6] The hydrogenation samples were prepared at 4 MPa with various temperatures: 252, 273, 295, and 563 K. The results showed that hydrogen-induced amorphization did not occur, but peak broadening was observed after the initial hydrogen absorption cycle. La_2Ni_7 gradually transformed into an amorphous state over ten hydrogen absorption−desorption cycles. Yartys et al. studied the crystal structure of $La_2Ni_7D_{6.5}$ using ex situ neutron diffraction,[7] and they reported that La_2Ni_7 maintains its crystal structure during absorption up to at least ~0.7 D/M. This corresponds to 65% of the maximum hydrogen content reported by Chung et al.[6] The structure of the full hydride phase is still unknown, and the hydrogen properties and structural changes in La_2Ni_7 have not yet been fully clarified.

*To whom correspondence should be addressed. E-mail: fbiwase@mx.ibaraki.ac.jp. Tel: +81-29-287-7189. Fax: +81-29-287-7189.

(1) Buschow, K. H. J.; Vanmal, H. H. *J. Less-Comm. Met.* **1972**, *29*, 203–210.
(2) Yamamoto, T.; Inui, H.; Yamaguchi, M.; Sato, K.; Fujitani, S.; Yonezu, I.; Nishio, K. *Acta Mater.* **1997**, 5213–5221.
(3) Zhang, D.-Y.; Tang, J.-K.; Gschneidner, K. A., Jr. *J. Less-Comm. Met.* **1991**, *169*, 45–53.
(4) Buschow, K. H. J.; Van Der Goot, A. S. *J. Less-Comm. Met.* **1970**, *22*, 419–428.
(5) Oesterreicher, H.; Clinton, J.; Bittner, H. *Mater. Res. Bull.* **1976**, *11*, 1241–1248.
(6) Chung, U. I.; Lee, J. Y. *J. Non-Cryst. Solids* **1989**, *110*, 203–210.
(7) Yartys, V. A.; Riabov, A. B.; Denys, R. V.; Sato, M.; Delaplane, R. G. *J. Alloys Compd.* **2007**, *408*−*412*, 273–279.

Published on Web 09/02/2010

Recently, Ce_2Ni_7-type alloys have attracted great interest as potential material for negative electrodes of nickel−metal hydride (Ni-MH) batteries. Yonezu et al. compared the electrochemical properties of a Ce_2Ni_7-type (Mm, $Mg)_2Ni_7$-related alloy and an $MmNi_5$-related alloy.[8] The (Mm, $Mg)_2Ni_7$ and $MmNi_5$-related alloys had discharge capacities of 340 and 310 mAh/g, respectively, with a charge and discharge current of 150 mA/g at 298 K. The discharge capacity of the $MmNi_5$-related alloy decreased by 60% from its initial capacity after 600 cycles, but that of the (Mm, $Mg)_2Ni_7$-related alloy reached 800 cycles with only 30% capacity loss. The results show that the (Mm, $Mg)_2Ni_7$-related alloy has a larger discharge capacity and better cycle stability than the $MmNi_5$-related alloy. This type of alloy has already been employed in some commercial Ni-MH batteries.[9]

Structural changes during hydrogenation provide substantial information for the development of hydrogen storage materials. For such alloys with superstructures, it is particularly interesting to elucidate how hydrogen occupies each $CaCu_5$- and $MgZn_2$-type cell during hydrogenation and how the hydrogen occupation of the cell is related to the hydrogenation properties. Some studies have reported the structural changes in Ce_2Ni_7-type alloys upon hydrogenation. Fillinchunk et al. reported the crystal structure of hydrogenated Ce_2Ni_7 using in situ synchrotron X-ray and neutron powder diffraction.[10] Their results showed that hexagonal Ce_2Ni_7 transformed into orthorhombic $Ce_2Ni_7D_{\sim 4}$. They indicated the differences in structural change between $Ce_2Ni_7D_{\sim 4}$ and a previously reported $La_2Ni_7D_{6.5}$ structure; Yartys et al. claimed that La_2Ni_7 maintained hexagonal symmetry ($P6_3/mmc$) even after hydrogenation. Although these two hydrides have different symmetries, they have similar hydrogen distributions in the stacking cells; most of the hydrogen occupies the $MgZn_2$-type cells, while the $CaCu_5$-type cells are almost empty.

This study focused on Ce_2Ni_7-type La_2Ni_7 to study the relation between hydrogenation properties and structural change. We attempted to observe hydrogen absorption−desorption phenomena and understand the structural changes from the alloy to the full-hydride phase (≥1.0 H/M) using in situ X-ray diffraction (XRD) along the $P-C$ isotherm. The structural parameters of the metal sublattice were refined using the Rietveld method, and the structural changes upon hydrogenation were analyzed. This study presents the phase transformation, lattice parameters, and volume of the $MgZn_2$- and $CaCu_5$-type cells with increasing hydrogen content, since the expanding behavior of $MgZn_2$- and $CaCu_5$-type cells should be closely related to the occupation of hydrogen in these cells.

2. Experimental Section

An La_2Ni_7 alloy was prepared by arc-melting La and Ni metals (99.9%) in an Ar atmosphere. The obtained ingot was annealed at 1153 K for 65 h under a vacuum of 2.0×10^{-2} Pa and quenched in ice water. The chemical composition was determined to be $La_2Ni_{7.5}$ by energy dispersive X-ray (EDX).

The sample for the $P-C$ isotherm measurement was sealed in a stainless steel container heated in vacuum at 373 K for 1 h and then evacuated at 273 K for 1 h. The $P-C$ isotherm was measured using the Sieverts method with no other pretreatment for activation.

The powder sample was sieved to a particle size of $<20\ \mu$m for XRD measurement. The crystal structure was determined through XRD using a Rigaku RINT 2500 V diffractometer equipped with a Bragg−Brentano-type goniometer. The operation conditions for the X-ray generator were 50 kV and 200 mA with 0.5° divergence and scattering slits and a 0.15 mm receiving slit. XRD data were obtained using Cu Kα radiation monochromatized with a curved graphite in a step-scan; the range of 2θ was 3−100° in ex situ measurements for the alloy and 19−95° in in situ measurements for the hydride phases.

XRD data was measured in situ using a high-pressure chamber with beryllium windows and a temperature-controlled sample stage attached to the goniometer. A 1.8 g sample was placed in a stainless steel holder and covered with a 0.5 mm-thick beryllium plate to maintain the surface flat of the sample during hydrogenation. The temperature was kept at 273 K after heating at 373 K for 1 h. To accurately evaluate the lattice parameters, NIST Si (640 C) was mixed with the sample as an internal standard. The peak shift due to shifting of the surface of the sample bed was also calibrated using the internal standard. Data at 2θ values around 51°, 71°, and 77°, which contained peaks from the beryllium plate, were excluded from refinement. BeO was included as the refinement as the second phase.

Possible space groups for the hydride phases were determined using the Dicvol06,[11] N-TREOR,[12,13] and EXPO 2004 packages.[14] Peak positions were determined after $K\alpha_2$-separation using EXPO2004, followed by indexing and refinement of the unit cell parameters. The structure parameters were refined with the Rietveld refinement program RIETAN-2000.[15−17] The pseudo-Voight function was used to express the peak profile, and the background intensity was fitted using a polynomial function with 12 parameters.

3. Results

3.1. Crystal Structure of La_2Ni_7. The XRD pattern of La_2Ni_7 in the 2θ region between 3° and 15° is shown in Figure 1. Two super-reflection peaks of the Ce_2Ni_7-type structure, 002 and 004, were clearly observed. The pattern also indicated that no La−Ni binary alloys with other superstructures, $PuNi_3$-, Gd_2Co_7-, or Pr_5Co_{19}-type, were contained in the sample. The observed 002 and 004 reflections corresponded to $d = 1.234$ and 0.617 nm, respectively, providing a value of about 2.47 nm for the lattice parameter c.

The structural parameters of the alloy were determined by Rietveld refinement of the XRD data in the 2θ region between 19° and 100°. Data at 2θ values around 30°, 34°, and 41°, which contained small peaks from an unknown

(8) Yonezu, I.; Yasuoka, S.; Fujitani, S. *Abstract of International Symposium on Metal-Hydrogen Systems* (*MH2008*), June 24−28, 2008, Reykjavik, Iceland.
(9) Murata, T.; Magari, Y.; Ishida, J.; Kihara, M.; Yasuda, S. *Sanyo Tech. Rev.* **2005**, *37*, 62–68.
(10) Filinchunk, Y. E.; Yvon, K.; Emerich, H. *Inorg. Chem.* **2007**, *46*, 2914–2920.
(11) Boultif, A.; Louer, D. *J. Appl. Crystallogr.* **2004**, *37*, 724–731.
(12) Altomare, A.; Giacovazzo, C.; Guagliardi, A.; Moliterni, A. G. G.; Rizzi, R.; Werner, P.-E. *J. Appl. Crystallogr.* **2000**, *33*, 1180–1186.
(13) Altomare, A.; Caliandro, R.; Camalli, M.; Cuocci, C.; Silva, I. D.; Giacovazzo, C.; Moliterni., A. G. G.; Spagna, R. *J. Appl. Crystallogr.* **2004**, *37*, 957–966.
(14) Altomare, A.; Burla, M. C.; Camalli, M.; Carrozzini, B.; Cascarano, G. L.; Giacovazzo, C.; Guagliardi, A.; Moliterni, A. G. G.; Polidori, G.; Rizzi, R. *J. Appl. Crystallogr.* **1999**, *32*, 339–340.
(15) Izumi, F. http://homepage.mac.com/fujioizumi/.
(16) Izumi, F. *Rigaku J.* **2000**, *17*(1), 34–45.
(17) Izumi, F.; Young, R. A. *The Rietveld Method*; International Union of Crystallography; Oxford University Press: Oxford, 1993, p 13.

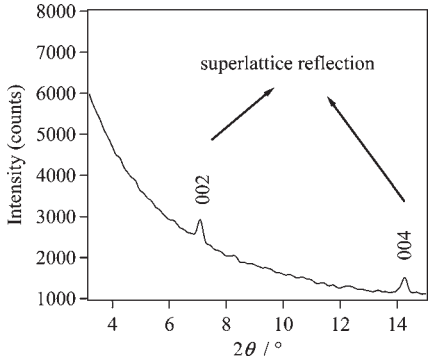

Figure 1. XRD pattern for La_2Ni_7 in a low-angle region. Superlattice peaks of 002 and 004 were observed.

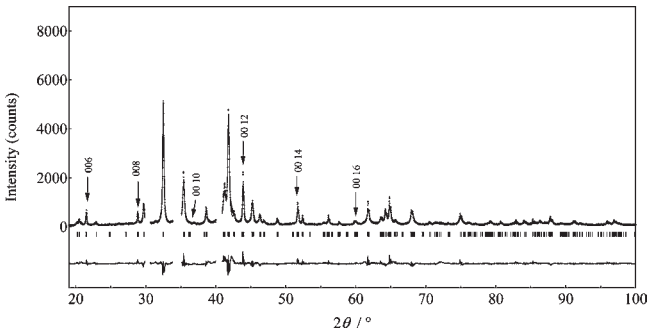

Figure 2. Refinement of XRD data for hexagonal La_2Ni_7. The line indicates calculated intensities, and the points superimposed on it are the observed intensities. The positions of Bragg peaks (bars) and the difference between the measured and calculated intensities are shown below the diffraction pattern.

phase and the Laves phase, were excluded from the refinement. Figure 2 shows the refined pattern of La_2Ni_7. The model was based on a Ce_2Ni_7-type structure with the space group $P6_3/mmc$. The refined lattice parameters a and c were 0.50656(9) and 2.4714(3) nm, respectively, which agreed with the values reported by Buschow and Van Der Goot.[4]

3.2. P−C Isotherm of La_2Ni_7. Figure 3 shows the $P-C$ isotherm of La_2Ni_7 at 273 K. The alloy absorbed hydrogen gradually up to 0.8 H/M and showed a plateau between 0.8 and 1.2 H/M. The absorption and desorption pressures for the plateau were 0.57 and 0.06 MPa, respectively. La_2Ni_7 showed larger hysteresis than $LaNi_5$. The maximum hydrogen storage capacity reached 1.24 H/M at 1.0 MPa. After the desorption measurement, 0.74 H/M of hydrogen remained.

3.3. Crystal Structure of Hydride Phase. Figure 4 shows in situ XRD patterns of the alloy and two hydride phases (the hydride phases I and II indicated in Figure 3). Their hydrogen contents were approximately 0.7 and 1.2 H/M, respectively. The pattern of phase I was clearly different from that of the alloy phase: the number of Bragg peaks observed for phase I was larger than that for the alloy phase. Small peaks from an impurity phase in the alloy sample disappeared upon hydrogenation due to amorphization. The pattern of phase II was similar to that of phase I, but the Bragg peaks shifted toward lower

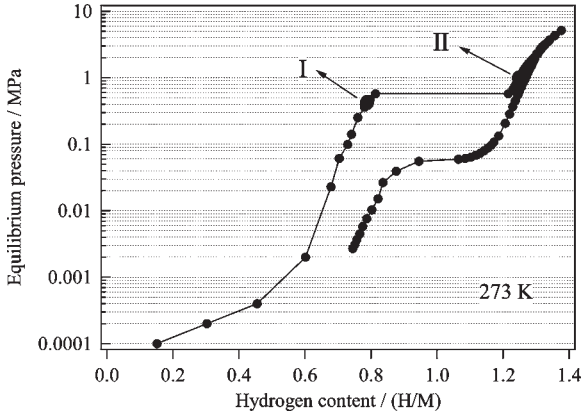

Figure 3. $P-C$ isotherm of La_2Ni_7 for the first absorption and desorption at 273 K.

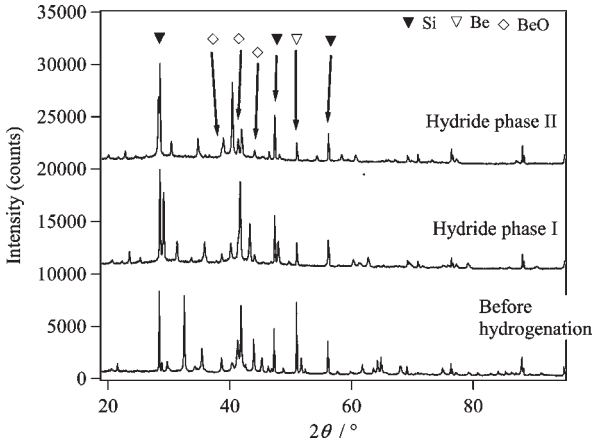

Figure 4. Change in XRD patterns for La_2Ni_7 during hydrogenation from the alloy phase to the hydride phases I and II. The patterns for the hydrides contain the diffraction of Si (internal standards), Be, and BeO (from a Be plate used for in situ measurements).

2θ values from phase I to phase II. Peak broadening was observed in both phases, but it was apparently smaller than that observed in $LaNi_5$.[18]

3.4. Crystal Structures of $La_2Ni_7H_{7.1}$ and $La_2Ni_7H_{10.8}$. An initial structural model of phase I based on the same space group as the $P6_3/mmc$ alloy was developed. The goodness of fit is defined as $S = R_{wp}/R_e$. The calculated pattern did not fit well with the observed pattern. The goodness of fit S was 7.76. The number of Bragg peaks for phase I was larger than that calculated for the structural model, indicating that the metal lattice changed from the space group $P6_3/mmc$ to lower symmetry during hydrogenation.

The 12 Bragg peaks for phase I were indexed using Dicvol06, which gave an orthorhombic unit cell with lattice parameters $a = 0.45$ nm, $b = 0.87$ nm, and $c = 3.03$ nm. They were indexed with EXPO as well, which gave possible symmetries matching space groups *Pnna*, *Pbcn*, *Pccn*, *Pbca*, or *Pnma* and lattice parameters $a = 0.50$ nm, $b = 0.86$ nm, and $c = 3.02$ nm. Both results indicated that the most possible symmetry for phase I was orthorhombic. The orthorhombic unit cell can be considered in relation to a hexagonal cell, as shown in Figure 6a, where the lattice parameters of the two structures are related to each other as $a_{orth} = a_{hex}$, $b_{orth} = 2\cos 30° a_{hex}$,

(18) Nakamura, Y.; Oguro, K.; Uehara, I.; Akiba, E. *J. Alloys Compd.* **2000**, *298*, 138–145.

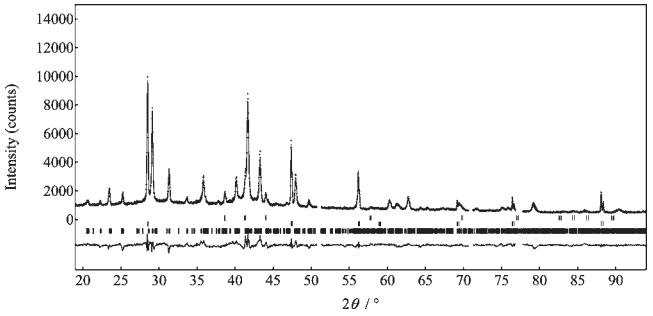

Figure 5. Refinement results of in situ XRD data for $La_2Ni_7H_{7.1}$. Upper, middle, and lower bars below the diffraction pattern indicate the positions of Bragg peaks for BeO, Si, and $La_2Ni_7H_{7.1}$, respectively.

and $c_{orth} = c_{hex}$. The simplest structure model would be based on an orthorhombic cell in which Ni atoms are located at the same positions as in the hexagonal structure for the alloy phase, as shown in Figure 6a. This possible simple lattice cannot be obtained using *Pnna*, *Pccn*, *Pbca*, and *Pnma*; only *Pbcn* satisfies the condition among the candidate space groups. The structural model for *Pbcn* contains two different La sites, La1 and La2, in 8*d* sites and eight different Ni sites, Ni1 at the 4*a* site, Ni3 at 4*c* site, and Ni2,4−8, at 8*d* sites. The structural parameters of phase I were determined by Rietveld refinement of the XRD data in the 2θ region between 19° and 95°. The pattern was refined using profile parameters, including both the anisotropic broadening parameters X_e (crystallite size) and Y_e (lattice strain) and isotropic parameters. The refined pattern is shown in Figure 5, and the refined structural parameters and the *R* factors are listed in Table 1.

EXPO suggested that the metal sublattice of phase II is monoclinic. A trial-and-error method for applying monoclinic structure models provided *C*2/*c*. The possible simple lattice could be obtained using *C*2/*c*. Refinement using the *C*2/*c* model provided $S = 2.08$. A satisfactory fit was obtained with space group *C*2/*c*. The refined structural parameters of phase II with *C*2/*c* were $a = 0.51641(9)$ nm, $b = 0.8960(1)$ nm, $c = 3.1289(1)$ nm, and $\beta = 90.17(1)°$, as shown in Table 2. The value of β was slightly larger than 90°. In order to confirm the *C*2/*c* model as the most probable model, we investigated higher symmetries. An orthorhombic *Pbcn* model has the closest structure to the *C*2/*c* model. The obtained lattice parameters for the *Pbcn* model excluding β were similar to *C*2/*c*; however, the *S* value of 2.52 was apparently larger. The *Pbcn* model did not fit as well as the orthorhombic models even with anisotropic peak broadening parameters. The deviation of β from 90° in the monoclinic symmetry was not negligible. As shown in Figure 7, the deviation induced the displacement of Ni1 atoms on the (001) plane by as much as 0.025 nm from the corresponding position in the orthorhombic model due to the large lattice parameter *c*, which was over 3.0 nm. The difference in the Ni1 atomic position between the orthorhombic and monoclinic models was significant. These results indicate that the most possible space group for phase II is *C*2/*c*. Figure 8 shows the Rietveld refinement pattern for phase II. The refined structural parameters are listed in Table 2. The crystal structure of phase II is illustrated in Figure 6c.

Table 1. Structural Parameters of $La_2Ni_7H_{7.1}$ (Phase I)[a]

atom	site	*g*	*x*	*y*	*z*	*B* (10^{-2} nm^2)
La1	8d	1.0	0.000(2)	0.329(4)	0.1845(1)	1.5(1)
La2	8d	1.0	0.000(2)	0.333(3)	0.0488(1)	3.4(2)
Ni1	4a	1.0	0	0	0	1.5(1)
Ni2	8d	1.0	0.542(9)	0.164(6)	0.1839(4)	1.2(4)
Ni3	4c	1.0	0	0.827(4)	1/4	1.9(5)
Ni4	8d	1.0	0.250(2)	0.118(3)	0.250(1)	0.9(2)
Ni5	8d	1.0	0.000(3)	0.800(2)	0.1098(4)	1.6(3)
Ni6	8d	1.0	0.313(5)	0.051(3)	0.1180(6)	1.5(4)
Ni7	8d	1.0	0.783(6)	0.075(5)	0.1049(4)	0.3(1)
Ni8	8d	1.0	0.000(2)	0.000(3)	0.1766(4)	1.5(2)

[a] Space group: *Pbcn* (No.60), $a = 0.50128(6)$ nm, $b = 0.8702(1)$ nm, and $c = 3.0377(1)$ nm. $R_{wp} = 6.41\%$, $R_I = 5.07\%$, $R_e = 3.08\%$, and $S = 2.08$.

Table 2. Structural Parameters of $La_2Ni_7H_{10.8}$ (Phase II)[a]

atom	site	*g*	*x*	*y*	*z*	*B* (10^{-2} nm^2)
La1	8f	1.0	0.000(2)	0.328(2)	0.3187(2)	1.6(2)
La2	8f	1.0	0.000(3)	0.322(3)	0.4548(1)	1.5(2)
Ni1	4a	1.0	0	0	0	1.7(3)
Ni2	8f	1.0	0.000(3)	0.000(4)	0.1771(5)	2.5(5)
Ni3	8f	1.0	0.000(4)	0.649(5)	0.1770(4)	1.4(1)
Ni4	8f	1.0	0.245(6)	0.592(5)	0.250(1)	0.7(5)
Ni5	4e	1.0	0.500(4)	0.324(4)	1/4	1.2(2)
Ni6	8f	1.0	0.500(3)	0.300(3)	0.1068(5)	1.3(4)
Ni7	8f	1.0	0.225(9)	0.560(6)	0.1095(6)	1.7(4)
Ni8	8f	1.0	0.749(8)	0.555(6)	0.1110(5)	0.9(3)

[a] Space group: *C*2/*c* (No.15), $a = 0.51641(9)$ nm, $b = 0.8960(1)$ nm, $c = 3.1289(1)$ nm, and $\beta = 90.17(1)°$. $R_{wp} = 6.31\%$, $R_I = 7.14\%$, $R_e = 3.14\%$, and $S = 2.01$.

4. Discussion

4.1. Crystal Structure. Yartys et al.,[7] using ex situ neutron diffraction, reported that $La_2Ni_7D_{6.5}$ has the same hexagonal symmetry ($P6_3/mmc$) as an alloy with lattice parameters $a = 0.49534(6)$ nm and $c = 2.9579(5)$ nm. This hydride seems to correspond to phase I in our study, considering the hydrogen content and lattice parameters. However, the observed in situ XRD pattern of phase I was apparently different from the pattern for an alloy with a hexagonal lattice. Rietveld refinement revealed that the metal sublattice of phase I was orthorhombic (space group: *Pbcn*). The structure of phase I, including the position of hydrogen (D), does not have symmetry any higher than this. Therefore, our results do not agree with those of Yartys et al.[7]

The structure of $Ce_2Ni_7D_x$ ($x = 4$ to 5) was studied by Fillinchunk et al.[10] and Denys et al.[19] Both studies indicated that Ce_2Ni_7 with a hexagonal structure ($P6_3/mmc$) transformed into $Ce_2Ni_7D_x$ with an orthorhombic structure (*Pmcn*). A similar structural change is observed for hydrogenation from La_2Ni_7 to $La_2Ni_7H_{7.1}$, although the symmetry of the hydride in both cases is not exactly the same.

Denys et al.[19] studied the phase transformation of Ce_2Ni_7 during deuteration using in situ neutron diffraction. The structure of $Ce_2Ni_7D_{4.7}$ was determined to be orthorhombic (*Pmcn*). The crystal structure of the metal sublattice of Ce_2Ni_7 transforms from hexagonal to orthorhombic in hydrogenation, as observed for La_2Ni_7

(19) Denys, R. V.; Yartys, V. A.; Sato, M.; Riabov, A. B.; Delaplane, R. G. *J. Solid State Chem.* **2007**, *180*, 2566–2576.

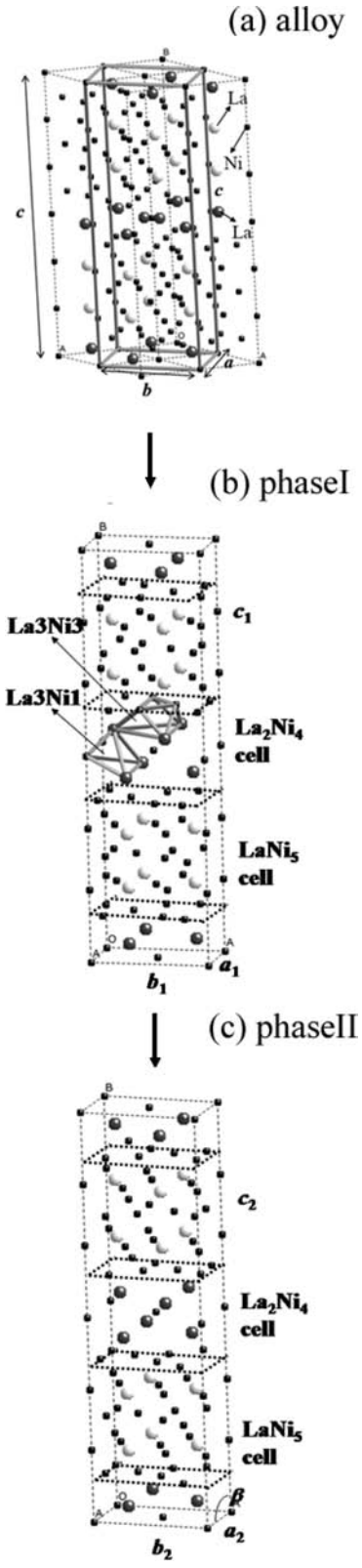

Figure 6. Structural changes in metal sublattice for La_2Ni_7: (a) before hydrogenation, (b) $La_2Ni_7H_{7.1}$ (phase I, orthorhombic), and (c) $La_2Ni_7H_{10.8}$ (phase II, monoclinic).

in this study. Refinement of $La_2Ni_7H_{7.1}$ (phase I) using the *Pmcn* model provided $S = 3.32$. The S value of the *Pmcn* model was apparently larger than that of the *Pbcn* model. The *Pmcn* model did not fit. In order to determine

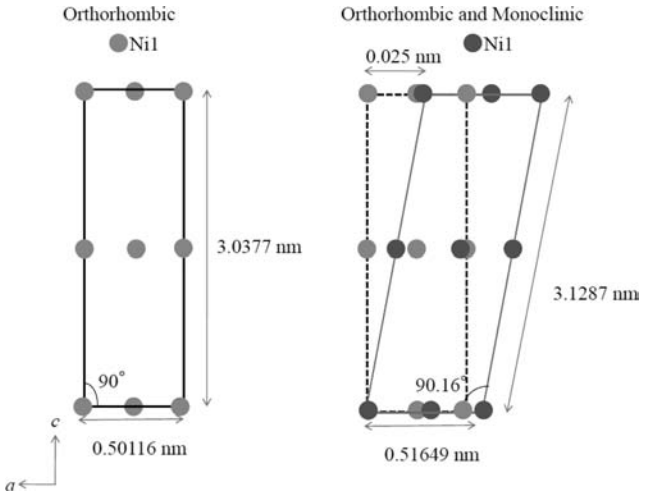

Figure 7. Position of the Ni1 atom in the orthorhombic and monoclinic structures projected along the <010> direction. Left: phase I (orthorhombic); right: phase II (orthorhombic and monoclinic).

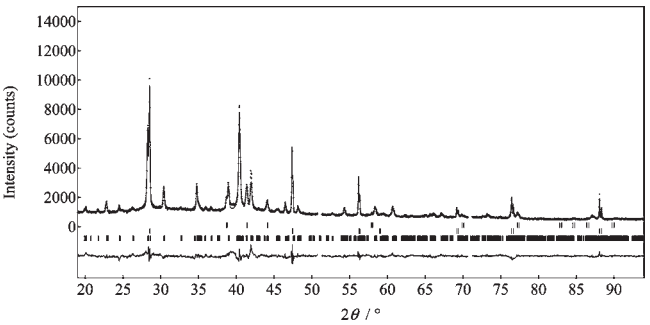

Figure 8. Refinement results of in situ XRD data for $La_2Ni_7H_{10.8}$. The upper, middle, and lower bars below the diffraction pattern indicate the positions of Bragg peaks for BeO, Si, and $La_2Ni_7H_{10.8}$, respectively.

Table 3. Expansion of the Lattice Axes, Unit Cell Volume, and the Volume of La_2Ni_4 and $LaNi_5$ Subunit[a]

	expansion 1 (%) alloy→phase I	expansion 2 (%) phase I→phase II	expansion 3 (%) alloy→phase II
a	−1.1	3.0	1.9
b	−0.8	3.0	2.1
c	22.9	3.0	26.6
unit cell volume	20.6	9.3	31.8
La_2Ni_4 cell volume	48.9	14.0	69.8
$LaNi_5$ cell volume	6.0	5.8	12.2

[a] Expansion 1 of phase I and expansion 3 of phase II were calculated using the value of the alloy as a reference. Expansion 2 of phase II was obtained from phase I.

the crystal structure of a hydride phase stable at a pressurized state, in situ measurement was necessary.

A hydride phase corresponding to $La_2Ni_7H_{10.8}$ in our study has not yet been reported in the literature. Our results revealed that the metal sublattice for phase II is monoclinic ($C2/c$).

4.2. Expansion of Unit Cell, $MgZn_2$- and $CaCu_5$-Type Subunit. The expansion of the axes and the unit cell is listed in Table 3. Here, the lattice parameters *a*, *b*, and *c* are defined as shown in Figure 6a for the alloy phase to evaluate the expansion of the three axes. The lattice

expanded anisotropically during transformation from the alloy to phase I: the *c* axis expanded by more than 20%, but the *a* and *b* axes shrank by about 1%, increasing the unit cell volume by 20%. In contrast, all of the axes expanded by 3% and the unit cell volume increased by 9% during transformation from phase I to phase II. The expansion rate per amount of absorbed hydrogen was similar to that for the formation of phase I.

The volume expansions of the La_2Ni_4 and $LaNi_5$ subunits were calculated as shown in Table 3. During the formation of phase I from the alloy, the La_2Ni_4 cell expanded by more than 48%, but the $LaNi_5$ cell expanded by only 6%. Both cells expanded by 5−14% during transformation from phase I to phase II. The cell expansion corresponds to the amount of hydrogen inserted into each of the La_2Ni_4 and $LaNi_5$ cells. Considering the expansion of each cell, most of the hydrogen occupied the La_2Ni_4 cells in phase I, with a small amount of hydrogen occupying the $LaNi_5$ cells. Hydrogen absorbed in the formation from phase I to phase II was likely to be distributed in both the La_2Ni_4 and $LaNi_5$ subunits, considering that both the cells expanded. The total volume expansion of the $LaNi_5$ cells was about 54% of that observed for $LaNi_5$ in the formation of $LaNi_5H_{\sim 7}$. Assuming that the $LaNi_5$ cell expanded in proportion to the hydrogen content for both $LaNi_5H_{\sim 7}$ and $La_2Ni_7H_{10.8}$, the hydrogen content in each $LaNi_5$ cell in $La_2Ni_7H_{10.8}$ seems to be about 0.4 H/M ($LaNi_5H_{\sim 2.4}$); around 30% of the total amount of hydrogen in $La_2Ni_7H_{10.8}$ is located in the $LaNi_5$ cell.

The expansions during the formation of phase I were compared with those reported for the formation of $Ce_2Ni_7D_{4.7}$.[19] The Ce_2Ni_4 cell expanded by 62−63%, but the volume of the $CeNi_5$ cell remained unchanged during hydrogenation. Rietveld refinement showed that hydrogen atoms were located only in the Ce_2Ni_4 cell. A study on $La_2Ni_7D_{6.5}$[7] reported the tendency for cell expansion and hydrogen occupation to be similar to those reported for $Ce_2Ni_7D_{4.7}$. There was a small difference in the expansion of the AB_5 cell between these reports (no expansion or shrinkage) and our study (expansion by 6%).

4.3. Hydrogen Sites Occupied in the $MgZn_2$- and $CaCu_5$-Type Subunit. The refined structural parameters and volume expansions showed that, in phase I, most of the hydrogen is located in the La_2Ni_4 cells. The structural changes to the orthorhombic symmetry form possible hydrogen sites at the center of the La_3Ni_3 octahedron and La_3Ni_1 tetrahedron in the La_2Ni_4 cell, as shown in Figure 6b. The volumes of the La_3Ni_3 octahedron and La_3Ni_1 tetrahedron increased by 35% and 135%, respectively, during hydrogenation. The La_2Ni_2 tetrahedron expanded by 34% in volume, and the expansion of three La_1Ni_3 tetrahedrons varied from 8% to 43%. The significantly large expansion of the La_3Ni_1 tetrahedron strongly suggests hydrogen occupation of this site in the La_2Ni_4 cell.

Partial occupation of hydrogen is possible in the La_3Ni_3 octahedron, La_2Ni_2 tetrahedron, and some of the La_1Ni_3 tetrahedrons. Denys et al.[19] reported that, for the Ce_2Ni_4 cell of $Ce_2Ni_7D_{4.4}$, hydrogen occupies the Ce_3Ni_1 tetrahedron, Ce_2Ni_2 tetrahedron, and Ce_3Ni_3 octahedron. The volumes for the Ce_3Ni_1 tetrahedron, Ce_2Ni_2 tetrahedron, and Ce_3Ni_3 octahedron increased by 170%, 26%, and 10%, respectively, during hydrogenation. The expansion of the Ce_3Ni_1 tetrahedron was larger than for the other sites. The same tendency was seen in the La_3Ni_1 tetrahedron for the La_2Ni_4 cell of La_2Ni_7. These results suggest that hydrogen occupation in La_3Ni_1 and Ce_3Ni_1 is associated with the phase transformation from hexagonal to orthorhombic. For the $LaNi_5$ cell, the volume change in four La_1Ni_3 tetrahedrons and three La_2Ni_2 tetrahedrons ranged from −15% to 34% and −2.0% to 14%, respectively.

The formation of phase II from phase I was accompanied by isotropic lattice expansion with volume increases of the La_2Ni_4 and $LaNi_5$ subunit, showing that hydrogen occupation in the subunit increased. For the La_2Ni_4 cell, the La_3Ni_3 tetrahedron expanded by 10% in volume, but two La_3Ni_1 sites were unchanged from phase I. The La_2Ni_2 tetrahedron expanded by 18%, and the volume of three La_1Ni_3 tetrahedrons changed from −23% to 61%. For the $LaNi_5$ cell, four La_1Ni_3 tetrahedrons showed volume changes from −7% to 17%, and three La_2Ni_2 tetrahedrons expanded from 14% to 38%. These results suggest that hydrogen remained in the La_3Ni_1 site and extra occupation occurred at some La_1Ni_3 sites in the La_2Ni_4 cell. Some of the La_2Ni_2 sites in the $LaNi_5$ cell are likely to be occupied. It is necessary to carry out in situ neutron diffraction to determine the hydrogen occupation for these hydride phases. The above results provide good suggestions for modeling the structure of the hydrides because, in most cases, the volume change in each site strongly reflects hydrogen occupation.

5. Conclusion

We investigated the phase transformation of La_2Ni_7 during hydrogenation through in situ XRD measurements along the *P*−*C* isotherm. The maximum hydrogen storage capacity reached 1.2 H/M in the first absorption, and about 60% of the maximum hydrogen capacity remained after the first desorption.

We found two hydride phases, $La_2Ni_7H_{\sim 7}$ and $La_2Ni_7H_{\sim 11}$, and determined the crystal structures of their metal sublattices. $La_2Ni_7H_{7.1}$ has an orthorhombic structure with space group *Pbcn*, and $La_2Ni_7H_{10.8}$ has a monoclinic structure with space group *C*2/*c*. The lattice expanded anisotropically during transformation from the alloy to $La_2Ni_7H_{\sim 7}$: the *c* axis expanded by more than 20%, but the *a* and *b* axes shrank by about 1%. The La_2Ni_4 cell expanded by 48%, but the $LaNi_5$ cell expanded by only 6%. Most of the hydrogen occupied the La_2Ni_4 cells in $La_2Ni_7H_{\sim 7}$, with a small amount of hydrogen occupying the $LaNi_5$ cells. During transformation from $La_2Ni_7H_{\sim 7}$ to $La_2Ni_7H_{\sim 11}$, all of the axes expanded by 3% and both the La_2Ni_4 and $LaNi_5$ subunit expanded by 5−14%, showing that hydrogen was distributed in the subunit. Considering expansion of tetrahedrons and octahedrons comprised by metal atoms, the La_3Ni_1 sites in the La_2Ni_4 cell are mainly occupied in $La_2Ni_7H_{\sim 7}$, and extra occupation at the La_1Ni_3 sites in the La_2Ni_4 cell and the La_2Ni_2 sites in the $LaNi_5$ cell are likely to be occupied in $La_2Ni_7H_{\sim 11}$.

Acknowledgment. Part of this work was supported by the New Energy and Industrial Technology Development Organization (NEDO) under "Advanced Fundamental Research on Hydrogen Storage Materials (HYDRO-STAR)".